AGU PUBLICATIONS

JGR

Journal of Geophysical Research: Biogeosciences

RESEARCH ARTICLE

10.1002/2013JG002592

Key Points:
- Drought-induced forest mortality is modeled using a stochastic framework
- Plant drought strategies are defined by soil and leaf hydraulic feedbacks
- Mortality is a threshold process linking plant, soil, and climate properties

Correspondence to:
A. J. Parolari,
anthony.parolari@duke.edu

Citation:
Parolari, A. J., G. G. Katul, and A. Porporato (2014), An ecohydrological perspective on drought-induced forest mortality, *J. Geophys. Res. Biogeosci.*, *119*, doi:10.1002/2013JG002592.

Received 6 DEC 2013
Accepted 19 APR 2014
Accepted article online 30 APR 2014

An ecohydrological perspective on drought-induced forest mortality

Anthony J. Parolari[1], Gabriel G. Katul[1], and Amilcare Porporato[2]

[1]Nicholas School of the Environment, Duke University, Durham, North Carolina, USA, [2]Department of Civil and Environmental Engineering, Duke University, Durham, North Carolina, USA

Abstract Regional-scale drought-induced forest mortality events are projected to become more frequent under future climates due to changes in rainfall patterns. The occurrence of these mortality events is driven by exogenous factors such as frequency and severity of drought and endogenous factors such as tree water and carbon use strategies. To explore the link between these exogenous and endogenous factors underlying forest mortality, a stochastic ecohydrological framework that accounts for random arrival and length of droughts as well as responses of tree water and carbon balance to soil water deficit is proposed. The main dynamics of this system are characterized with respect to the spectrum of anisohydric-isohydric stomatal control strategies. Using results from a controlled drought experiment, a maximum tolerable drought length at the point where carbon starvation and hydraulic failure occur simultaneously is predicted, supporting the notion of coordinated hydraulic function and metabolism. We find qualitative agreement between the model predictions and observed regional-scale canopy dieback across a precipitation gradient during the 2002–2003 southwestern United States drought. Both the model and data suggest a rapid increase of mortality frequency below a precipitation threshold. The model also provides estimates of mortality frequency for given plant drought strategies and climate regimes. The proposed ecohydrological approach can be expanded to estimate the effect of anticipated climate change on drought-induced forest mortality and associated consequences for the water and carbon balances.

1. Introduction

Drought-induced forest mortality events are now recognized as a global phenomenon with consequences for large-scale water and carbon cycling [*Allen et al.*, 2010]. Under the prospect of increased frequency and severity of drought [*Schneider et al.*, 2007], the capability to predict the likelihood of such events and their consequences for carbon-water cycling has become imperative. To date, considerable progress has been made toward a predictive framework that accounts for the causes and mechanisms of drought-induced forest mortality. However, beyond the myriad complexities associated with modeling the soil-plant system [*Katul et al.*, 2007], this modeling work is still limited by uncertainty associated with the physiological mechanisms that lead to mortality during severe drought [*McDowell et al.*, 2008; *Sala et al.*, 2010; *McDowell et al.*, 2011, 2013].

Several drought-induced mortality mechanisms have been proposed, including hydraulic failure, carbon starvation, and biotic attack. Mortality may occur when either water, carbon, or both is depleted below the level(s) necessary to support physiological processes. Further, water and/or carbon deficit may increase susceptibility to insect or pathogen outbreaks (e.g., growth-differentiation balance theory [*Herms and Mattson*, 1992]), which can also cause widespread mortality [*McDowell et al.*, 2013]. Despite the trade off between growth and defense, recent experimental evidence suggests forest resilience during drought and drought-induced forest mortality are strongly related to tree carbon balance and hydraulic function as well as climatic conditions [*McDowell et al.*, 2008; *Sala et al.*, 2010; *McDowell*, 2011; *Anderegg et al.*, 2012; *Mitchell et al.*, 2013; *McDowell et al.*, 2013; *Clifford et al.*, 2013].

As an alternative to predicting the outcome of individual droughts, the approach used in the studies cited above, the relation between drought and mortality may also be addressed by estimating the likelihood, or frequency, of drought-induced mortality. The frequency of drought-induced forest mortality events depends on the interaction between endogenous factors such as plant water and carbon use strategies and exogenous factors such as soil and climate properties that determine water and carbon availability. Together, soil, climate, and resource use strategies regulate the intensity, duration, and frequency of

©2014. American Geophysical Union. All Rights Reserved.

"physiological drought" [*Mitchell et al.*, 2013]—the condition of either water or carbon deficit. The role of climate in water availability is primarily characterized by the timing and amount of rainfall events that recharge root zone soil moisture and by evaporative demand. Between rainfall events, plant water and carbon use strategies impact soil moisture utilization and carbon acquisition rates, which are primarily coupled through stomatal transport. Diagnoses of drought-induced forest mortality must therefore account for the statistics of drought, i.e., the random arrival and volume of rainfall, as well as the plant-controlled response of ecosystem water and carbon use during drought.

In this paper, a statistical-dynamical model of the soil-plant water and carbon balances is proposed to estimate the frequency of drought-induced forest mortality. The soil type, vegetation water and carbon use strategies, and climate characteristics that contribute to hypothesized mortality mechanisms are present but minimally represented. Plant drought response is formulated as a multivariable feedback control system, where ecosystem water use, carbon uptake, and respiration interact simultaneously with soil moisture and plant hydraulic status. In this new approach, the soil moisture dynamics, conditioned by climate and ecosystem water use, serve as the basis for plant hydraulic regulation, carbon balance, and the frequency of drought-induced mortality.

2. Model

The modeling approach introduced below consists of a dynamical system that couples the soil-plant water balance and plant carbon balance and is forced by stochastic precipitation. In section 2.1, plant resource use strategies are discussed in terms of transpiration sensitivity to soil water deficit, which provides a basis for the model assumptions. In sections 2.2 and 2.3, the equations describing water and carbon depletion during drought are introduced. Finally, section 2.4 defines the assumptions for the stochastic precipitation forcing. Model symbols and units are listed in Table 1.

2.1. Plant-Water Feedback

The effect of drought on plant water use can be characterized as a negative feedback between surface saturation (i.e., soil moisture, plant tissue water potential, and air relative humidity) and the outgoing water flux, transpiration. Transpiration depletes water stored in soil and plant tissues, and as this water is depleted, transpiration subsequently decreases. This negative feedback can be partly attributed to physical limits to the water supply under dry conditions. That is, large negative water potentials in soil or xylem cause cavitation represented macroscopically by a reduced liquid water conductance. Plant physiological adjustments also contribute to this feedback. Plants have adapted a variety of physical and physiological mechanisms that regulate transpiration during drought, including stomatal control and plasticity of root, xylem, and canopy function [*Magnani et al.*, 2002; *Sperry*, 2004; *Brodribb and McAdam*, 2011]. This physiologically mediated feedback has many possible adaptive advantages, including the maintenance of adequate leaf hydration for photosynthesis, cavitation avoidance, and soil water conservation.

Stomatal control is one component of the plant drought response that has been studied extensively and linked to drought-induced mortality [*McDowell et al.*, 2008; *Mitchell et al.*, 2013]. Therefore, it offers an instructive example for formulating a model of plant water feedback. Stomatal aperture is directly controlled by changes in turgor pressure of epidermal and guard cells. However, the mechanisms linking environmental perturbations to corresponding changes in turgor are currently deliberated [e.g., *Buckley*, 2005; *Nikinmaa et al.*, 2013; *Pantin et al.*, 2013]. Despite this uncertainty, two general signals are commonly presumed to explain how stomata sense the soil water state. First, changes in xylem water supply or atmospheric water demand affect the local energy balance and hydraulic status within and near the guard cells and epidermis [*Buckley*, 2005]. Second, a biochemical signal is produced in roots and shoots and transported to guard cells. This biochemical signal may involve abscisic acid production [*Tardieu et al.*, 1993, 1996], changes in pH or other sap constituents [*Davies et al.*, 2002], or aquaporin activity [*Vandeleur et al.*, 2009]. Leaf, xylem, and soil hydraulic states induce active regulation of guard cell osmotic pressure, which causes stomata to close when the internal or external environment dries.

The relative strength of the leaf and soil hydraulic signals produces variability in the stomatal response to drought. Stomatal control strategies are generally described across a spectrum of drought sensitivity. At one end of this spectrum, isohydric species close stomata rapidly under drought conditions such that leaf water potential is regulated within a narrow range. This behavior limits xylem cavitation but simultaneously reduces carbon uptake. At the other end of the spectrum, anisohydric species maintain open stomata

©2014. American Geophysical Union. All Rights Reserved.

Table 1. Model Symbols and Units

Variable or Parameter	Units	Symbol
Relative soil moisture	-	s
Relative plant water content	-	w
Soil-to-plant water flux	mm d^{-1}	E_s
Plant-to-atmosphere water flux	mm d^{-1}	E_a
Additional water loss term	mm d^{-1}	L
Soil porosity	-	n
Root zone depth	mm	z_r
Plant capacitance	-	c
Maximum soil-root-plant conductance	mm d^{-1}	g_{srp}
Maximum stomatal conductance	mm d^{-1}	g_s^{max}
Time-varying environmental forcing	-	$\phi(t)$
Vapor pressure deficit	-	D
Soil moisture feedback gain	-	k_s
Plant hydraulic feedback gain	-	k_w
Wilting point	-	s_w
Equilibrium point	-	s_e
Maximum additional water loss rate	mm d^{-1}	K_s
Nonstructural carbohydrate (NSC) concentration	g C	C
Photosynthesis	g C d^{-1}	P
Growth	g C d^{-1}	G
Growth respiration	g C d^{-1}	R_g
Maintenance respiration	g C d^{-1}	R_m
Maximum assimilation rate	g C d^{-1}	A_{max}
Maximum transpiration rate	mm d^{-1}	E_{max}
Canopy water demand to soil-root-plant supply ratio	-	β
Sensitivity of w to s	-	δ
Soil moisture time constant	d	$\tau = (1 - s_e)\eta^{-1}$
Normalized maximum soil moisture loss rate	-	η
Plant water content threshold at hydraulic failure (HF)	-	w_c
Steady state NSC	g C	C_0
Soil moisture at point of NSC consumption	-	s_0
NSC threshold at carbon starvation (CS)	g C	C_c
Time to reach s_0	d	t_{s_0}
Time to reach C_c	d	t_{C_c}
Critical soil moisture at mortality	-	$s_c = \max(s_{\mathrm{HF}}, s_{\mathrm{CS}})$
Critical drought length at mortality	d	t_{CS} or t_{HF}
Drought-induced mortality rate	d^{-1}	ν_m
Normalized soil moisture loss function	d^{-1}	ρ
Soil moisture probability density function	-	p
Frequency of rainfall events	d^{-1}	λ
Mean rainfall depth	mm	α

during drought. This behavior promotes carbon uptake at the expense of decreased leaf water potential and potential extensive xylem cavitation. Therefore, isohydric species are more susceptible to negative carbon balance and carbon starvation, whereas anisohydric species are more susceptible to cavitation and total hydraulic failure [*McDowell et al.*, 2008; *Mitchell et al.*, 2013; but see *McDowell*, 2011]. This spectrum of water use strategies offers a tantalizing link between physiology and climate in the occurrence of mortality [*Kumagai and Porporato*, 2012].

While the complete physiological response to drought involves numerous adjustments that span diurnal to multiyear time scales, the detailed understanding of stomatal control suggests two necessary elements of a minimal model of plant water feedback. First, plants sense environmental stimuli that vary at fast (i.e., solar radiation, humidity, and leaf water potential) and slow (i.e., soil moisture) time scales. Second, plant functional types vary in the sensitivity of transpiration to these environmental signals. That is, the isohydric-anisohydric spectrum can be interpreted as a spectrum of environmental sensitivity, where isohydric species exhibit the strongest plant water feedback and anisohydric species the weakest. These general features of plant drought response are incorporated into the model now discussed.

©2014. American Geophysical Union. All Rights Reserved.

2.2. Plant-Soil Water Balance

A two-compartment representation of the soil-plant water balance is used to describe the coupled dynamics of soil moisture, s, and relative plant water content, w,

$$nz_r \frac{ds}{dt} = -E_s(s,w) - L(s), \tag{1a}$$

$$c \frac{dw}{dt} = E_s(s,w) - E_a(s,w), \tag{1b}$$

where n ($m^3\ m^{-3}$) is the soil porosity, z_r (mm) is the active root depth, c (mm) is the plant tissue capacitance, E_s (mm d^{-1}) is the soil water supply that transports liquid water from the soil to the leaves, E_a (mm d^{-1}) is the atmospheric water demand that transports water vapor from the leaves into the atmosphere, and $L(s)$ (mm d^{-1}) is an additional loss term. $L(s)$ represents soil moisture losses competing with transpiration, including bare soil evaporation, leakage, and root water uptake by neighboring plants. The soil-leaf water flux is given by

$$E_s(s,w) = \begin{cases} 0 & s < s_w \\ g_{srp}(s-w) & s_w \le s \le 1 \end{cases}, \tag{2}$$

where g_{srp} (mm d^{-1}) is the maximum soil-root-plant conductance and s_w is the wilting point, which will be defined later. Similarly, the leaf-atmosphere flux is

$$E_a(s,w) = g_s^{max} \phi(t) D u(s,w), \tag{3}$$

where g_s^{max} (mm d^{-1}) is the maximum stomatal conductance, $\phi(t)$ (–) is a time-varying environmental forcing that accounts for diurnal fluctuations in radiation, temperature, and humidity, D (–) is the vapor pressure deficit, and $u(s,w)$ (–) is the stomatal control function.

The function $u(s,w)$ encodes key aspects of the physiological control strategy. It represents the regulation of stomatal aperture in response to the two system states, s and w. The following expression is assumed,

$$u(s,w) = \begin{cases} 0 & s < s_w \\ 1 - k_s(1-s) - k_w(1-w) & s_w \le s \le 1 \end{cases}, \tag{4}$$

where k_s and k_w are the control parameters or the sensitivity of stomatal conductance to the soil or plant water status, respectively. From a control systems perspective, these coefficients are labeled as the "feedback gains" [*Stengel*, 1994; *Bechhoefer*, 2005]. This form of u has two important features. First, in the absence of plant control (i.e., $k_s = k_w = 0$ and $u = 1$), the stomata are locked in the open position with conductance $g_s^{max}\phi(t)$. Second, when the plant actively controls its stomata (i.e. $k_s > 0$ and/or $k_w > 0$), stomatal conductance decreases with either decreasing s or w or both. As a logical starting point to accommodate such active controls, equation (4) combines these two feedbacks linearly, whereas other studies have assumed more elaborate nonlinear forms [e.g., *Tardieu et al.*, 1996].

The term $L(s)$ represents an additional loss term that combines the influence of bare soil evaporation, leakage, and competition from neighboring plants. $L(s)$ has a maximum K_s (mm d^{-1}) and declines linearly with decreasing s as

$$L(s) = K_s u(s,w). \tag{5}$$

Physically, K_s can be interpreted as the rate of soil moisture depletion under well-watered conditions due to processes outside the control of the tree species of interest.

Equation (1) may be solved analytically for $s(t)$ and $w(t)$ by time scale separation. For most plants, w stabilizes much quicker than s, resulting from the larger soil water storage capacity, nz_r, relative to the plant tissue storage, c. Therefore, the time variation of $w(t)$ can be approximated as a series of steady states superimposed over $s(t)$, denoted $\hat{w}(t)$. To maintain analytical tractability, it is assumed that $\phi(t) = 1$. The details of this solution are presented in Appendix A, whereas the main results are discussed in section 3 below.

©2014. American Geophysical Union. All Rights Reserved.

2.3. Nonstructural Carbohydrates

The availability of nonstructural carbohydrates (NSC) to support maintenance respiration during drought is an important but poorly constrained component of the drought response. This is particularly true for isohydric species that tightly regulate gas exchange and rely on stored carbohydrates during dry periods. A generic mass balance for NSC storage (denoted C below) is [*Amthor and McCree*, 1990; *McDowell*, 2011]

$$\frac{dC}{dt} = P - G - R_g - R_m, \tag{6}$$

where P, G, R_g, and R_m represent photosynthesis, growth of structural tissues, and growth and maintenance respiration, respectively. Each of these carbon fluxes decreases as drought develops, albeit at different rates. According to the parameterization of *Amthor and McCree* [1990], the dynamics of C occur in three phases. Under well-watered conditions, photosynthesis is sufficient to support growth and respiration. Surplus carbon is diverted to storage, and if the well-watered period is sufficiently long, C reaches a steady state. Under mild drought, growth decreases more quickly than photosynthesis, causing a slight increase in C. Under severe drought, growth and photosynthesis decrease rapidly to zero, while maintenance respiration declines more slowly. This shift in the plant carbon balance leads to C depletion and eventual mortality if entirely consumed.

To comply with an analytical treatment (in particular, the stochastic analysis below), this model of C is conceptualized as a two-phase process. First, under well-watered conditions, C is maintained at its steady state value, C_0, which serves as the initial state prior to a prolonged drought. Second, when soil moisture crosses below a critical value s_0, growth ceases and C is consumed at a constant respiration rate, r (g C d^{-1}). Photosynthesis under water stress is linked to the plant water use strategy, $u(s, w)$, which regulates stomatal aperture and, thus, CO_2 supply. A constant water use efficiency is assumed, WUE $= A_{max}/E_{max}$, where A_{max} (g C d^{-1}) is the maximum rate of photosynthesis and E_{max} is the maximum transpiration rate, equal to $g_s^{max}D$. This assumption is equivalent to ignoring variations in intercellular CO_2 concentration (c_i) with increased drought stress. While this assumption is questionable, changes in c_i impact photosynthesis much less than the decline in stomatal conductance with stress. Therefore, with these assumptions, when soil moisture is below the threshold s_0 and in the absence of rainfall, C decays according to

$$\frac{dC}{dt} = P - r = A_{max}u(s, w) - r, \tag{7}$$

where r accounts for maintenance respiration, $G = 0$ and $R_g = 0$.

2.4. Precipitation

Precipitation events are modeled as a stochastic process with arrivals following a Poisson process with mean storm frequency λ (d^{-1}). Precipitation event depths are assumed to be independently and identically exponentially distributed with mean depth α (mm). The soil water balance subject to this forcing has been previously studied in detail [*Rodriguez-Iturbe et al.*, 1999; *Laio et al.*, 2001; *Porporato et al.*, 2001; *Rodriguez-Iturbe and Porporato*, 2004], and the relevant solutions are repeated in Appendix A for completeness.

3. Plant Water Use Strategies

A wide spectrum of plant water use strategies is predicted by the model introduced above. These strategies are characterized by the volume of available soil moisture, the rate at which this water is consumed, and the relative homeostasis of leaf water potential. These characteristics and their dependence on climate, soil, and vegetation parameters are discussed in the following section.

3.1. Water Balance Stability

The wilting point, s_w, is a common parameter in hydrological models that defines the soil moisture value at which transpiration ceases [*Rodriguez-Iturbe and Porporato*, 2004]. Under severe water deficit, transpiration may be limited by reduced stomatal conductance, xylem transport capacity, or root water uptake. Soil moisture stored below s_w cannot be extracted by the vegetation, and therefore, s_w also controls the maximum volume of plant available water, which for our model is $nz_r(1 - s_w)$. Because transpiration reaches zero at s_w, we define s_w in terms of the equilibrium point of the model (i.e., $ds/dt = 0$, which implies $E_a = u = 0$),

$$s_e = 1 - \frac{1}{k_s + k_w}. \tag{8}$$

©2014. American Geophysical Union. All Rights Reserved.

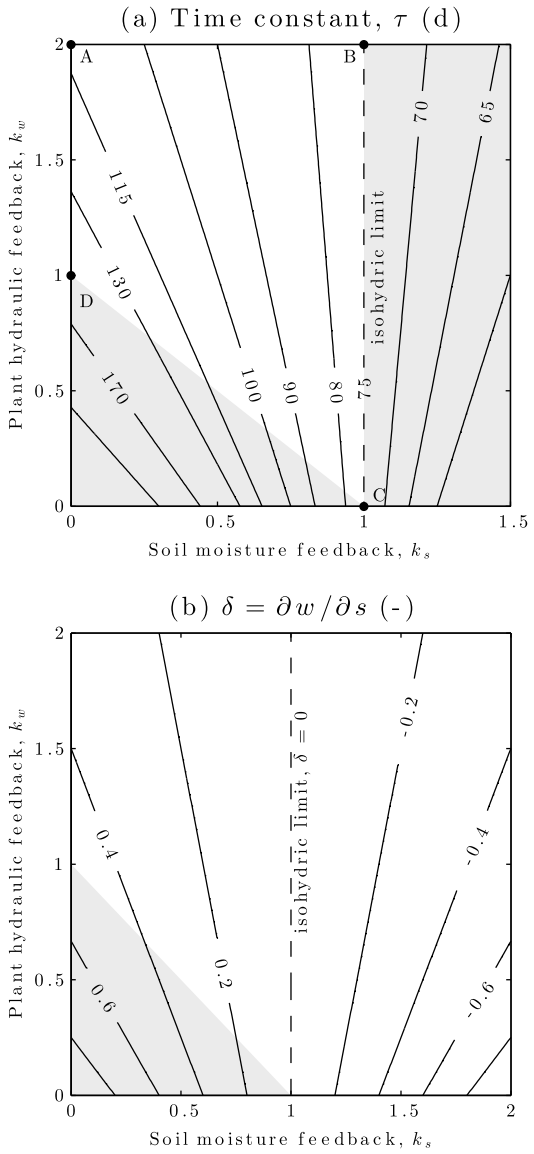

Figure 1. Plant-soil water balance parameters: (a) time constant, τ (day), and (b) sensitivity of $w(t)$ to $s(t)$, δ (–), as a function of the soil moisture and plant hydraulic feedback gains. Viable plant water use strategies are those associated with concurrent drying of the plant and soil media (i.e., $\partial w/\partial s > 0$). Strategies with a negative equilibrium point (i.e. $s_e < 0$ and $s_w = 0$) are marked by the gray triangles. For this example, $\beta = 1$, $E_{max} = 3$ mm d^{-1}, $n = 0.45$, and $z_r = 50$ cm. See section 3 for a description of end-member points A–D.

Restricting s_w to the physically meaningful range $0 \le s_w \le 1$, this definition leads to

$$s_w = \max\left(0, 1 - \frac{1}{k_s + k_w}\right), \tag{9}$$

which depends on the sum of the control parameters and provides an appropriate bound for equations (2) and (4). Equation (9) accommodates a range of water use strategies.

The limits of equation (8) are associated with infeasible water use strategies. As $k_s + k_w$ increases, $s_w \to 1$. This limit represents the most conservative water use strategy. Stomatal closure responds to drought so rapidly that no water is transpired, stored soil moisture is entirely available to other losses, and photosynthesis is severely inhibited. For plants with completely rigid stomata (i.e., $k_s = k_w = 0$), $s_e = -\infty$. That is, the plant and the soil dry indefinitely. In reality, plant and soil drying continues until the point at which physical limits to water transport and turgor maintenance become important. For example, the stomata of plants lacking active stomatal control mechanisms, such as lycophytes and ferns [*Brodribb and McAdam*, 2011], close passively in response to low epidermal turgor [*Buckley*, 2005; *Brodribb and McAdam*, 2011]. Equation (9) imposes these physical limits as a threshold at $s = 0$. There is likely a restricted range of $k_s + k_w$ associated with viable plant water use strategies.

Between these limits, s_w stabilizes at a finite value less than 1. In this range, equation (9) is consistent with the isohydric-anisohydric strategy spectrum. Gas exchange in anisohydric species is less sensitive to drought (i.e., low $k_s + k_w$), leading to low s_w, high plant available moisture, and high transpiration and photosynthesis rates. On the other hand, isohydric species are characterized by high $k_s + k_w$, high s_w, and low transpiration and photosynthesis rates. Equation (9) also states that there is a minimum level of feedback required to maintain $s_w > 0$. This requirement is $k_s + k_w > 1$, as indicated by line CD in Figure 1. As will be seen in section 4 below, the viability of a given s_w depends on its value relative to the point of hydraulic failure in the soil-plant-atmosphere continuum and the point of NSC depletion.

3.2. Water Balance Dynamics

In addition to s_w and plant available moisture, the plant water use strategy also plays a role in the time variability of s and $\hat{w}$ during drought. This role is primarily expressed through the interaction of s and $\hat{w}$, which impacts the driving force for transpiration, $s - \hat{w}$, and thus the actual rate of water use. The coupled plant and soil water balance dynamics are described below by two quantities dependent on the plant water use strategy: the soil water balance time constant approximating the residence time of water in the soil system,

©2014. American Geophysical Union. All Rights Reserved.

τ, and the sensitivity of $\hat{w}$ with respect to s, $\delta = \partial\hat{w}/\partial s$. The soil moisture time constant, τ, senses the effective rate at which soil moisture is being depleted by evapotranspiration and all other losses, while δ senses the depletion of $\hat{w}$ for a given s, which contributes to the fraction of total evapotranspiration partitioned to transpiration versus storage. Both parameters depend on a combination of soil, plant, and atmosphere characteristics, including the relative contributions of k_s and k_w. Expressions for τ and δ are derived in Appendix A.

For values of s where plants are active (i.e., $s_w \leq s \leq 1$), the soil moisture time constant is the sum of the contributions from transpiration, E, and other losses, L,

$$\tau = \left(\frac{\eta}{1 - s_e}\right)^{-1} = \left[\frac{K_s + E_{\max}(1 + \beta k_w)^{-1}}{nz_r(1 - s_e)}\right]^{-1}, \tag{10}$$

where $E_{\max} = g_s^{\max} D$ and $\beta = E_{\max} g_{\mathrm{srp}}^{-1}$. The contribution of the control strategy to τ is the ratio of the maximum transpiration rate, $E_{\max}(1 + \beta k_w)^{-1}$, to maximum plant available moisture, $nz_r(1 - s_w)$, where the distinct effects of k_s and k_w on the soil water balance are now explicit. The primary role of k_s is to modulate the wilting point. Increased sensitivity to the soil moisture signal always decreases plant available moisture, transpiration rate, and the time of positive gas exchange (i.e., when $u > 0$). k_w has the same effect on s_w but plays a secondary role in determining the maximum transpiration rate through the factor $(1 + \beta k_w)^{-1}$. Increased sensitivity to the plant hydraulic signal decreases plant available moisture and the maximum transpiration rate under well-watered conditions.

With this background, the spectrum of water use strategies whose characteristics depend on the relative strengths of the two environmental feedback mechanisms is now explored. In general, this is a two-dimensional strategy landscape (i.e., k_s and k_w), where plant activity is defined by the available water volume and the water utilization rate (Figure 1). Plants range from the most aggressive water users (point C, low s_w, and high E) to the most conservative water users (point B, high s_w, and low E). Defined in this way, aggressive water users rely less on environmental information generated by fluctuating leaf water potentials, whereas conservative water users rely on a combination of leaf water potential and the gradual recession of soil moisture. The line AB corresponds to the minimum transpiration rate; the line BC corresponds to the isohydric limit where $\beta^{-1}k_s = 1$; and the line CD corresponds to the maximum plant available moisture. At point C, the feedback is generated entirely by soil moisture, and the plant achieves the maximum plant available water and maximum transpiration rate.

The derived expression for δ is

$$\delta = \frac{\partial\hat{w}}{\partial s} = \frac{1 - \beta k_s}{1 + \beta k_w}. \tag{11}$$

This quantity effectively translates $s(t)$ to $\hat{w}(t)$, thereby controlling relative hydraulic homeostasis. If a perfectly isohydric strategy is defined as that which maintains $\hat{w}(t)$ constant, or $\mathrm{d}\hat{w}/\mathrm{d}t = 0$ for all finite values of t, this requires $\delta = 0$. Therefore, perfectly isohydric plants are associated with either of the following conditions:

$$k_s = \beta^{-1}, \qquad k_w \to \infty. \tag{12}$$

If $k_w \to \infty$, transpiration goes to zero (i.e., $E_s \to 0$), which is not a viable strategy. Further, δ is more sensitive to k_s than k_w (Figure 1). It can then be surmised that the soil moisture feedback is a practical requirement for perfectly isohydric stomatal regulation and an efficient mechanism for achieving nearly isohydric behavior. Condition (12) also suggests that the level of feedback associated with isohydric behavior is linked with the soil, vegetation, and climate properties that determine the balance between soil water supply and atmosphere water demand, encapsulated in β.

3.3. Diurnal Variations in *w*

Evaporative demand varies diurnally as the result of coupled variations in solar insolation, temperature, and relative humidity. This behavior can be idealized by a sinusoidal function with period $T = 1$ d,

$$\phi(t) = \sin(2\pi t) + 1 \tag{13}$$

©2014. American Geophysical Union. All Rights Reserved.

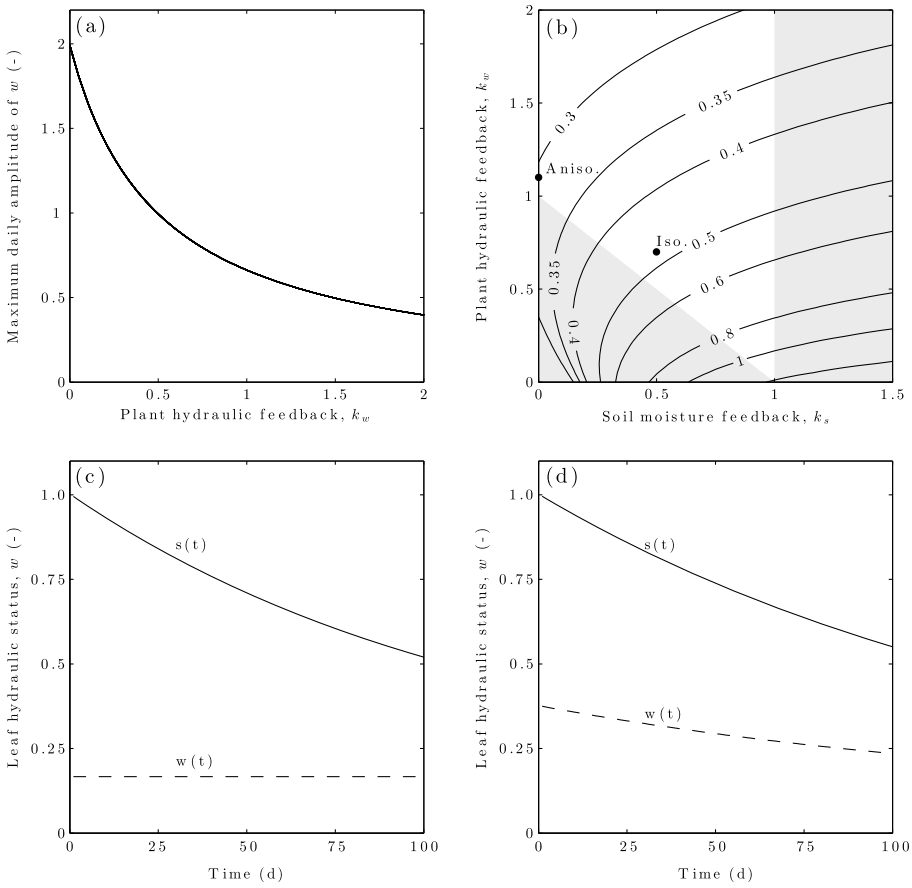

Figure 2. The effect of the soil moisture and plant hydraulic feedback gains on the soil-leaf saturation gradient, $s - w$: (a) the maximum gradient under well-watered conditions and (b) the dynamic range of $s - w$ over a 100 day drought. Examples of diurnal w variations for (c) isohydric and (d) anisohydric strategies, corresponding to the points in the top right (solid lines: s, dashed lines: w).

so that $\phi(t)$ is always positive and the time average $\overline{\phi(t)} = 1$. The time-varying conductance ratio is then

$$\beta(t) = \frac{E_{\max}}{g_{\mathrm{srp}}}\phi(t) = \beta\phi(t). \tag{14}$$

With this assumption, the system is now a linear, first-order ordinary differential equation with periodic coefficients that can be solved numerically.

Based on these solutions, the roles of soil moisture and leaf hydraulic signals can be further distinguished. The transpiration rate is controlled by soil-xylem conductance and the soil to leaf water potential gradient (here modeled as $s - w$). Independent of k_s, k_w controls the diurnal variability of w on any given day (Figure 2a). Therefore, the effect of k_w on τ results from a modulation of the soil-leaf hydraulic gradient. The dynamic range of $s - w$ between days, on the other hand, is controlled by k_w and k_s (Figure 2b). For the same total feedback, $k_s + k_w$, the hydraulic gradient increases with the relative contribution of k_s (Figure 2b). This suggests that the soil moisture signal can increase plant available moisture, particularly under wet conditions, while regulating w under dry conditions. The leaf hydraulic state is thus necessary to regulate midday w, and information on the soil moisture state may be used in combination to provide a wider range of control throughout the drydown.

Lastly, it can be shown that this periodic system has an analog to the isohydric criterion (equation (12)),

$$k_s = [2\beta]^{-1}. \tag{15}$$

This result is similar to equation (12) but now reflects the fact that the conductance ratio has a diurnal maximum 2β at midday. The strategy is therefore defined by the midday w, the diurnal minimum.

©2014. American Geophysical Union. All Rights Reserved.

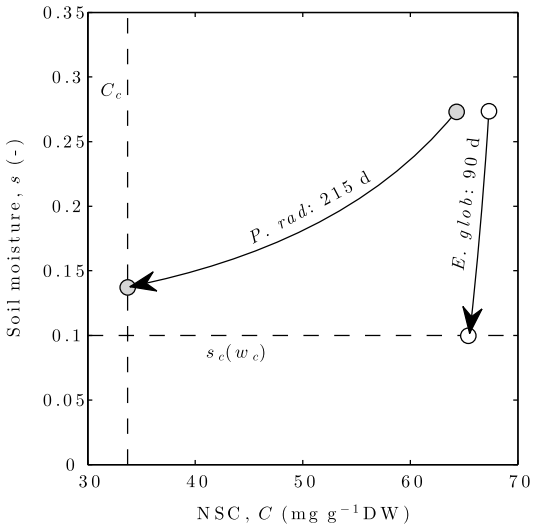

Figure 3. Measured (symbols) and modeled (solid lines) soil moisture and nonstructural carbohydrate dynamics for the drought-induced mortality experiment reported by *Mitchell et al.* [2013]. The dashed lines correspond to the critical thresholds of the inferred mortality mechanism for each species: C_c is the carbon starvation threshold for *P. radiata* and $s_c(w_c)$ is the hydraulic failure threshold for *E. globulus*. For *P. radiata*, $k_s = 0.52$, $k_w = 0.59$, and $r = 0.15$ mg NSC g^{-1} DW d^{-1}. For *E. globulus*, $k_s = 0$, $k_w = 0.77$, and $r = 0.038$ mg NSC g^{-1} DW d^{-1}. Common parameters are $E_{max} = 4$ mm d^{-1}, $n = 0.45$, $z_r = 122$ mm, $\beta = 1$, and $r/A_{max} = 0.5$.

4. Resource Use Strategies and Drought-Induced Mortality

Within the confines of the model proposed here, the occurrence of a drought-induced plant mortality event depends on plant water use strategy and the carbon balance. In this section, the model is used to delineate critical soil moisture states at which either mortality mechanism, hydraulic failure (HF) or carbon starvation (CS) (or both), occurs. The soil water balance dynamics then provide an estimate of the typical drought length required to induce a mortality event. The model is applied to a controlled greenhouse drought experiment. We do not consider diurnal variability in $\phi(t)$ for this analysis.

4.1. Critical Soil Moisture Threshold and Drought Length

Under the assumption that drought-induced mortality occurs by either HF or CS, the key system properties are resource availability (i.e., either water or carbon) and the rates at which these resources are consumed. Mortality is assumed to occur when one of two critical resource availability thresholds is crossed, due to the fact that physiological processes, such as xylem water transport or photosynthesis, are irreparably impaired beyond these thresholds. For HF, this threshold corresponds to a critical value of $\hat{w}$, $\hat{w}_c$, where xylem tension is lost and water transport ceases. For CS, this threshold corresponds to a critical value of C, C_c, where accessible nonstructural carbohydrates are exhausted and respiratory energy can no longer be generated. These critical plant states are now translated to the soil water balance to compute an analogous soil moisture threshold, $s_c = \max(s_{CS}, s_{HF})$.

The value of s_{HF} is calculated from the quasi steady state equation for $\hat{w}(t)$ (equation (A1)),

$$s_{HF} = \delta^{-1}\left[\hat{w}_c + \frac{\beta(1 - k_w - k_s)}{1 + \beta k_w}\right], \tag{16}$$

which depends on the control strategy (k_s, k_w). The time to reach s_{HF} from an arbitrary initial condition $s(t = 0) = s_i$, in the absence of rainfall, is then given by the dynamic equation for $s(t)$ (equation (A5)),

$$t_{HF} = -\tau \ln\left(\frac{s_{HF} - s_e}{s_i - s_e}\right). \tag{17}$$

Here s_i is a specified model parameter, but it can be generally interpreted as the soil moisture immediately following an arbitrary rainfall/infiltration event. Therefore, with randomly varying rainfall input, s_i is itself a random variable whose distribution will depend on climate, soil, and vegetation properties.

To calculate s_{CS}, it is necessary to calculate the threshold s_0 below which consumption begins (see section 2.3). A plausible starting point is to assume s_0 is crossed when respiratory costs are balanced by photosynthetic carbon gain. Therefore, equation (7) is set equal to 0 and solved to obtain

$$s_0 = \frac{r}{A_{max}(k_s + k_w\delta)} + s_e, \tag{18}$$

where s_0 depends on both the water use strategy, through $k_s + k_w\delta$, and the carbon use strategy, characterized by r/A_{max}.

Beyond this point, C decays according to equation (7). The time required for the plant to completely exhaust available NSC can be computed as (see Appendix B)

$$t_{C_c} = \frac{\Delta C + A_{max}(k_s + k_w\delta)(s_0 - s_e)\tau}{r}, \tag{19}$$

©2014. American Geophysical Union. All Rights Reserved.

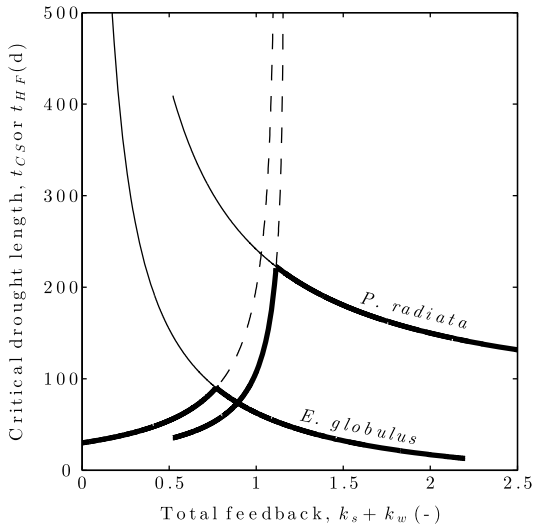

Figure 4. Critical drought length for carbon starvation (thin solid lines) and hydraulic failure (dashed lines) as a function of the total stomatal feedback to plant-soil saturation, $k_s + k_w$. For *P. radiata* and *E. globulus*, $k_s = 0.52$ and $k_s = 0$, respectively, while k_w is varied. The thick solid line indicates the minimum drought length required to induce mortality, beginning from $s_i = 0.27$. The maximum survival time is the point where $t_{CS} = t_{HF}$.

where $\Delta C = C_0 - C_c$ is the available NSC. Therefore, the critical soil moisture threshold for CS is

$$s_{CS} = (s_0 - s_e)\exp\left(-t_{C_c}/\tau\right) + s_e. \quad (20)$$

Also, the time to reach s_{CS} starting from s_i is

$$t_{CS} = t_{s_0} + t_{C_c} = -\tau \ln\left(\frac{s_0 - s_e}{s_i - s_e}\right) + t_{C_c}. \quad (21)$$

This is the sum of the time from s_i to s_0 and the time from s_0 to s_{CS}, the former of which is obtained from the soil moisture dynamics (see Appendix A).

These expressions demonstrate the interaction between climate (E_{max}), soil (n, z_r, β), and the plant water and carbon use strategy (k_s, k_w, w_c, A_{max}, r, and ΔC). As modeled, these factors determine the relative depletion rates of available water and carbon, which subsequently govern the drought-induced mortality time scale. This point is investigated further through the case study below.

4.2. Case Study: Response of *E. globulus* and *P. radiata* to Controlled Drought

The model is now applied to interpret the drought-induced mortality experiment reported by *Mitchell et al.* [2013]. In this experiment, 100 individuals each of *Eucalyptus globulus* (Blue Gum) and *Pinus radiata* (Radiata Pine) were subjected to a terminal drought. *E. globulus* is characterized as an aggressive water user, with a typically anisohydric strategy, whereas *P. radiata* is characterized as a conservative water user, with a typically isohydric strategy. During the experiment, *E. globulus* suffers a complete loss of xylem conductivity, indicative of runaway cavitation, and minimal depletion of NSC reserves after 90 days. On the other hand, *P. radiata* maintains xylem conductivity, has generally lower leaf gas exchange throughout the drought, and utilizes approximately 50% of NSC reserves at death after 215 days. Hence, this experiment serves as a logical case study for the proposed model, as it fixes climate and soil while varying the two primary drivers of mortality: (1) resource availability (i.e., NSC or s) and (2) resource use strategy.

The carbon and water use trajectories, as well as the observed critical drought length, are captured by the model (Figure 3). Parameters were estimated from the experimental data as follows. Measurements of predawn leaf water potential were transformed to relative soil moisture assuming a sandy loam with porosity $n = 0.45$, air entry pressure $\psi_b = -1.47 \times 10^{-3}$ MPa, and retention exponent $b = 4.38$. E_{max}, k_s, and k_w were calibrated using soil moisture and transpiration measured by weight. Note that the calibrated $k_s + k_w = 0.77 < 1$ for *E. globulus*, indicating a negative $s_e = -0.30$, while the hydraulic failure threshold was estimated as $s_c = 0.10$ (Figure 3). Respiration rates were estimated from NSC measurements at the beginning of the drought and after death. The thresholds for carbon starvation and hydraulic failure were assumed to coincide with measured NSC and soil moisture values at death, respectively. We assumed $r/A_{max} = 0.5$ and $\beta = 1$ as reasonable values for both species.

The model predicts a maximum critical drought length when the xylem cavitation and accessible NSC thresholds are crossed simultaneously (Figure 4). These threshold crossings are controlled by the stomatal control strategy or the total feedback $k_s + k_w$. Rapid stomatal closure (i.e., high $k_s + k_w$) increases the time to hydraulic failure, by regulating plant hydraulic status within functional limits, but decreases the time to carbon starvation, by limiting CO_2 supply. Therefore, there exists an optimal $k_s + k_w$, at which $t_{CS} = t_{HF}$, that maximizes survivable drought length.

The optimal critical drought length and its location along the feedback axis depends on resource availability, as characterized by total accessible carbohydrates and soil moisture. Based on the experimental measurements, *P. radiata* is able to sustain a high respiration rate for the duration of the drought, whereas

©2014. American Geophysical Union. All Rights Reserved.

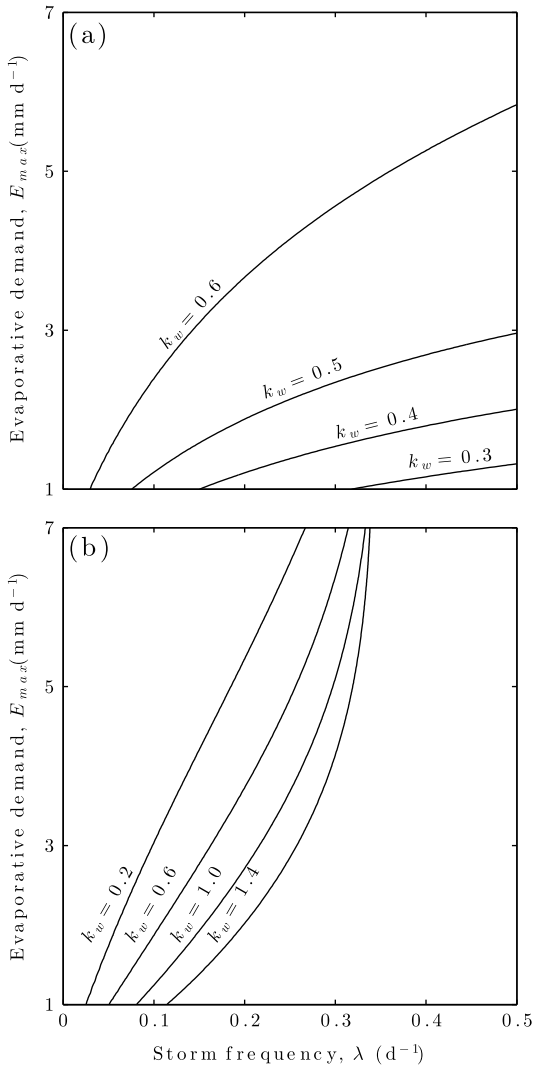

Figure 5. The dependence of drought-induced mortality frequency on the stomatal control strategy for (a) hydraulic failure and (b) carbon starvation. The contours indicate lines of equal frequency, $\nu_m^{-1} = 50$ years. The upper left corner corresponds to the driest climate; therefore, mortality is more frequent above the lines and less frequent below. Climate is characterized by the maximum evaporative demand, E_{max}, and mean storm frequency, λ. The mean storm depth, α, is varied coincidentally so as to maintain constant mean annual rainfall ($P = 540$ mm for a 180 d wet season). The stomatal control strategy is characterized by $k_s = 0.5$ and several values of k_w. The xylem cavitation threshold is $\hat{w}_c = 0.1$, and the carbon starvation threshold is $\Delta C = 15$ mg C g^{-1} DW.

E. globulus utilizes very little NSC. On the other hand, *E. globulus* draws soil moisture to a lower level before catastrophic xylem cavitation occurs. *P. radiata* mortality occurs at 215 days, whereas *E. globulus* mortality occurs much earlier at 90 days. The difference in NSC availability is the primary reason for the shorter critical drought in *E. globulus*, while the increased soil moisture availability only partly compensates (Figure 4).

The coordination of carbohydrate storage and acquisition with xylem and phloem transport may have a mechanistic basis (see reviews by *McDowell* [2011] and *McDowell et al.* [2011]). NSC availability for respiratory consumption may be limited by competing sinks, such as osmotic adjustment or embolism repair, that improve hydraulic function. Further, excessive cavitation may reduce NSC transport, isolating storage from energy-demanding processes. Phloem carbohydrate concentrations may also play a direct role in turgor pressure and stomatal response [*Nikinmaa et al.*, 2013]. The physical coupling between NSC and water availability underlying the plant drought response is minimally accounted for by the heuristic parameterization used here. Resource thresholds, C_c and $\hat{w}_c$, integrate those processes leading to the disruption of resource accessibility, whereas k_s and k_w integrate both hydraulic and osmotic triggers for stomatal closure. One adaptive benefit of coupled carbon balance and hydraulic function is suggested here—the most resilient plant drought survival strategy is that which navigates the *C-s* phase space (Figure 3) such that no resources are left unused at the point of mortality.

5. Drought-Induced Forest Mortality Rate

In the previous section, the model was used to estimate the survivable drought length and to elucidate the key physiological parameters contributing to drought resilience. The soil water balance subject to a stochastic rainfall forcing is now revisited to estimate the frequency, or rate, of drought-induced mortality events given a plant resource use strategy and climate characteristics. In addition to considering general plant-climate relationships, this approach is applied to the 2000–2003 western United States drought as a discussion point for qualitative comparison.

5.1. Drought-Induced Mortality Rates Derived From Climate Statistics

The drought-induced mortality rate, ν_m (d^{-1}), is defined as the average number of mortality events per unit time. Alternatively, the reciprocal of ν_m is the average time between drought-induced mortality events. Below, ν_m is estimated by forcing the model described above with stochastic rainfall (section 2.4). Therefore, ν_m incorporates the statistical distributions of drought, imposed by the climate forcing, and the dynamic

©2014. American Geophysical Union. All Rights Reserved.

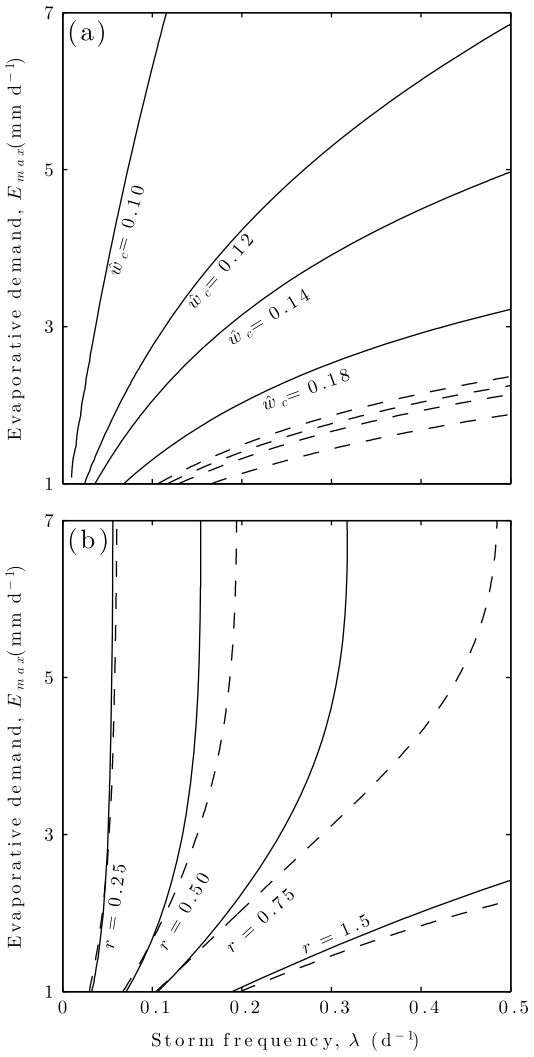

Figure 6. The dependence of drought-induced mortality frequency on climate and plant water and carbon use strategies for (a) hydraulic failure and (b) carbon starvation. The contours indicate lines of equal frequency, $\nu_m^{-1} = 50$ years. The upper left corner corresponds to the driest climate; therefore, mortality is more frequent above the lines and less frequent below. Climate is characterized by the maximum evaporative demand, E_{max}, and mean storm frequency, λ. The mean storm depth, α, is also varied so as to maintain a constant annual rainfall, ($P = 540$ mm for a 180 d wet season). The plant water use strategy is characterized by xylem cavitation resistance, w_c, and stomatal feedback (isohydric, (k_s, k_w)=(0.52,0.59), solid lines; anisohydric, (k_s, k_w)=(0,0.77), dashed lines), and the carbon use strategy by the respiration rate, r. All other parameters are those for *P. radiata*.

vegetation drought response, defined by the water and carbon use strategies. This ν_m is analogous to the time scales previously defined in section 4.1. However, under stochastic rainfall forcing, ν_m accounts for the entire sequence of alternating wet and dry periods prior to the threshold crossing.

Drought-induced mortality is assumed to occur whenever s crosses below either of the mortality thresholds s_{CS} and s_{HF}, defined in equations (16) and (20). The mortality rate ν_m is then the average frequency of such crossings when the soil moisture process is at steady state. The frequency of crossing below a specified value of s was previously derived as

$$\nu_m = \nu_{s_c} = \rho(s_c)p(s_c), \tag{22}$$

where $s_c = \max(s_{CS}, s_{HF})$ is the critical soil moisture value, $\rho(s_c)$ (d^{-1}) is the normalized soil moisture loss function evaluated at s_c, and $p(s_c)$ [–] is the soil moisture probability density function evaluated at s_c [*Porporato et al.*, 2001]. In Appendix A, $\rho(s)$ and $p(s)$ are given.

How ν_m varies with resource availability, resource use strategy, and climate is now considered. Here climate is characterized by maximum evaporative demand, E_{max}, which may be considered a proxy for vapor pressure deficit, and the mean frequency of rainfall events, λ. Annual rainfall is held constant by simultaneously varying the mean storm depth α. For illustrative purposes, a feasible drought-induced mortality rate is assumed to be on the order of once per 50 years. That is, we assume a given strategy is viable in a given climate if mortal drought occurs every 50 years or less frequently. Note that for some parameter combinations, ν_m may not have a unique solution as a function of the climate parameters. In these cases, we take the ν_m associated with the wetter climate, where the soil moisture dynamics primarily occur above the mortality threshold. Although the mortality threshold may be crossed at the same frequency in a drier climate, we assume that soil moisture conditions are too dry to support the population.

The modeled relationship between drought resilience strategy and climate is complex and suggests coordination between the stomatal control strategy (k_s, k_w), cavitation vulnerability ($\hat{w}_c$), and carbon balance ($A_{max}, \Delta C, r$). The model predicts isohydric and anisohydric stomatal control strategies can be viable across a wide range of climates, given sufficient coordination with cavitation vulnerability and respiration rate (or other components of metabolism). As expected from the model dynamics, and from the previous prediction of an optimal tolerable drought length, increased stomatal sensitivity to drought (i.e., more isohydric) confers protection against HF in arid climates but increases susceptibility to CS (Figure 5). Further, lower stomatal sensitivity (i.e., more anisohydric) to drought requires a lower cavitation vulnerability to avoid HF in arid climates (Figure 6a).

©2014. American Geophysical Union. All Rights Reserved.

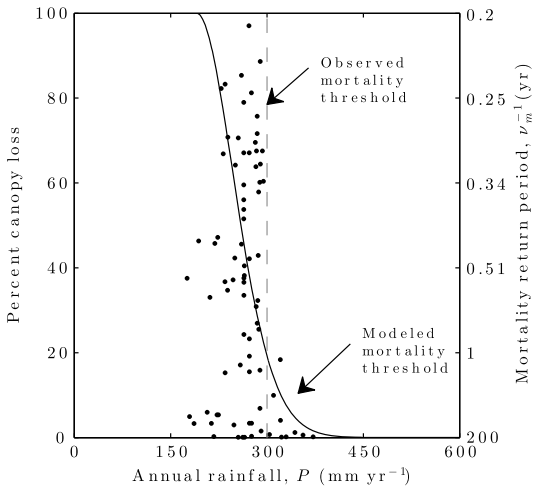

Figure 7. Comparison of observed percent pinyon pine canopy loss during the early 2000s drought (black dots) and modeled mortality frequency (solid line) as a function of precipitation. The data points correspond to observations made in 95 plots, 100 m^2 in area sampled between 2005 and 2008 [*Clifford et al.*, 2013]. NSC reserves are chosen such that carbon starvation and hydraulic failure are predicted to occur simultaneously. Observed annual rainfall refers to the average over the 2 year period 2002–2003, whereas the modeled annual rainfall refers to the product $P = \alpha\lambda T_{seas}$, where $T_{seas} = 180$ d is the wet season length. Parameters are the same for *P. radiata* except $z_r = 1$ m, $\beta = 1.25$, and $\hat{w}_c = 0.145$.

With respect to CS, the relative performance of isohydric and anisohydric strategies across climates varies widely. Assuming the same NSC balance parameters, isohydric and anisohydric strategies are associated with similar mortality rates by CS in climates characterized by infrequent, high-intensity rainfall or by low evaporative demand (Figure 6b). These climates correspond to those with long-duration or low-intensity droughts, respectively. In contrast, anisohydric strategies are predicted to experience higher CS frequency than isohydric strategies in climates with frequent, low-intensity rainfall and high evaporative demand, corresponding with short, high-intensity drought. Similar to HF, this discrepancy can be mitigated by lower respiration rates in anisohydric species. The largest variation in NSC dynamics would therefore be expected in these climates. These modeling results highlight the importance of a multifactor drought resilience strategy as well as the sensitivity of these strategies to rainfall variability, irrespective of the climatic mean rainfall.

Owing to their contrasting stomatal behaviors, it may be speculated that isohydric species are more prevalent in climates characterized by short-duration, high-intensity droughts, whereas anisohydric species are more prevalent in climates characterized by long-duration, low-intensity droughts [*McDowell et al.*, 2008; *Kumagai and Porporato*, 2012; *Mitchell et al.*, 2013]. *Kumagai and Porporato* [2012] confirmed this hypothesis and also showed that anisohydric species may be preferred in humid climates due to higher gas exchange. However, their model only considered mortality by HF, whereas our model also includes a minimal representation of the plant carbon balance and mortality by CS. Interestingly, isohydric and anisohydric strategies do coexist, such as in the Pinyon-Juniper woodlands of the southwestern United States [*McDowell et al.*, 2008]. In addition to coordination of the stomatal control strategy with other physiological traits, this may also result from interannual climate variability that differentially favors either strategy.

5.2. Case Study: Percent Canopy Loss of *P. edulis* Across a Rainfall Gradient During a Multiyear Drought

Widespread *Pinus edulis* (pinyon pine) die-off occurred in the southwestern United States following a multiyear drought during the period 2000–2003 [*Breshears et al.*, 2005]. Tree mortality during this event was attributed to low precipitation, increased temperatures, and bark beetle infestation. Plot-level and remotely sensed observations of percent canopy loss across a rainfall gradient in New Mexico suggest a threshold precipitation below which substantial die-off occurred [*Clifford et al.*, 2013].

The model predictions are qualitatively similar to this threshold response of die-off to precipitation. The model predicts a rapid increase in the frequency of drought-induced mortality with decreasing precipitation (Figure 7). For average conditions, the likelihood of mortality rises from almost nonexistent to near certainty over a narrow range of annual precipitation. Given the typically isohydric behavior of the pinyon pine [*McDowell et al.*, 2008], the modeled frequency of drought-induced mortality increases from once every 50 years to once every year as the climatic average precipitation falls from 425 mm/yr to 315 mm/yr. That is, the frequency of fatal drought increases by 50 times for a 20% decrease in annual rainfall. This result suggests an extremely tenuous relationship between plant strategies and climate.

Because multiple forest mortality events have not been (and likely never will be) observed under field conditions, the modeled drought-induced mortality frequency, ν_m, is difficult to validate. The observations

©2014. American Geophysical Union. All Rights Reserved.

reported by *Clifford et al.* [2013] offer a natural experiment that lends some confidence to the approach proposed here. This model-data comparison is best viewed as a space-for-time substitution whereby mortality risk is (a) simulated by a sequence of droughts corresponding to a marked Poisson process and (b) observed in the field as a series of time-coincident droughts corresponding to spatial heterogeneity in precipitation and other factors. While the data do not support estimation of ν_m values directly, it does verify the existence of a drought threshold that induces mortality and can be approximately modeled by precipitation. The modeling approach proposed here takes the additional step of linking precipitation to the plant strategy through the soil water balance, thereby providing an ecohydrological mortality threshold.

6. Conclusion

This work introduced a methodology for linking drought statistics with plant drought survival strategies to estimate the frequency of drought-induced mortality events. The model delineates the relative roles of soil moisture and leaf hydraulic signals underlying the isohydric-anisohydric water use strategy spectrum in the context of drought-induced mortality. These strategies are shown to interact with other properties of the soil-plant-atmosphere system in determining the frequency of drought-induced mortality events and the range of suitable climates for a given strategy. The model exhibits a maximum tolerable drought length, achieved by coordination between available carbon and water resources. Further, the model predicts that increased mean drought length, a potential consequence of global change [*Schneider et al.*, 2007], will increase drought-induced mortality rates for extant species, irrespective of changes in total annual precipitation.

The model employs several assumptions to allow analytical tractability. In particular, the plant carbon balance is reduced to well-watered, constant NSC and drought-stressed NSC consumption conditions. Further, the respiration rate is assumed constant, whereas the carbon costs of survival may increase as the drought length increases (as reviewed by *McDowell et al.* [2011]). With respect to the water balance, the soil-plant hydraulic pathway and stomatal control functions rely on macroscale states intended to aggregate a wide range of microscale processes [e.g., *Katul et al.*, 2007]. Finally, mechanistic interactions between NSC availability and xylem transport capacity beyond the effect of stomatal aperture were ignored, at least within the context of determining critical drought conditions resulting in a mortality event.

Drought-induced forest mortality is an emerging aspect of global change, and adequate predictive tools are required to quantify the risk and impact of these events. While some of the mechanisms explored here have been implemented in dynamic global vegetation models, many questions remain open [*McDowell et al.*, 2011, 2013]. We have addressed one outstanding issue by analyzing plant resource strategies in the context of a randomly varying climate to quantify physiological drought and the frequency of drought-induced mortality at climatic time scales.

Appendix A: Solution to the Coupled Soil-Plant Water Balance

In Appendix A, the coupled soil-plant water balance described in equations (1)–(5) is solved. In addition, the steady state soil moisture probability density function associated with this system is presented.

A1. Temporal Dynamics of $s(t)$ and $\hat{w}(t)$

To obtain the quasi steady state $\hat{w}(t)$ in terms of $s(t)$, assume $w(t)$ is at steady state with respect to the slow time scale of $s(t)$. Then, setting equation (1b) equal to 0 implies $E_a = E_s$, and from equations (2) and (3), $\hat{w}$ can be expressed in terms of s,

$$\hat{w}(t) = \delta s(t) - \frac{\beta(1 - k_w - k_s)}{1 + \beta k_w} \tag{A1}$$

where

$$\delta = \frac{\partial \hat{w}}{\partial s} = \frac{1 - \beta k_s}{1 + \beta k_w}, \tag{A2}$$

$\beta = g_s^{\max} D g_{srp}^{-1}$ is the canopy water demand to soil-xylem water supply ratio and $\hat{w}$ denotes the quasi steady state value of w.

©2014. American Geophysical Union. All Rights Reserved.

With $\hat{w}$ defined entirely in terms of s, the system dynamics can be obtained by integrating the appropriate dynamic equation for s. Plugging equation (A1) into equation (2) and combining with equations (1a) and (5), the following equation is obtained:

$$\frac{ds}{dt} = -\rho(s) = \begin{cases} 0 & s < s_w \\ -\eta\left[\frac{s(t)-s_e}{1-s_e}\right] & s_w \le s \le 1 \end{cases}, \tag{A3}$$

where

$$\eta = \frac{1}{nz_r}\left(\frac{E_{\max}}{1+\beta k_w} + K_s\right) \tag{A4}$$

and $E_{\max} = g_s^{\max} D$. In (A3), $s_e = 1 - (k_w + k_s)^{-1}$ is the steady state of equations (1a) and (1b), and the wilting point is restricted to positive values of s, $s_w = \max\left(0, s_e\right)$. This equation has the solution

$$s(t) = (s_i - s_e)\exp\left(-t/\tau\right) + s_e, \tag{A5}$$

where $s_i = s(t=0) > s_w$ is the initial condition and the time constant for $s(t)$ is

$$\tau = \left(\frac{\eta}{1-s_e}\right)^{-1} = \left[\frac{K_s + E_{\max}(1+\beta k_w)^{-1}}{nz_r(1-s_e)}\right]^{-1}. \tag{A6}$$

Combining equations (A1) and (A5) gives

$$\hat{w}(t) = \delta(s_i - s_e)\exp\left(-t/\tau\right) + s_e. \tag{A7}$$

The time from s_i to any value of s can be obtained directly from equations (A5) and (A7).

A2. Probability Density Function for s, $p(s)$

In this section, we now consider the soil water balance, given by equation (A3), forced by precipitation events, $P(t)$, modeled as a stochastic process. This approach is detailed in *Rodriguez-Iturbe et al.* [1999], *Laio et al.* [2001], and *Rodriguez-Iturbe and Porporato* [2004], and the important assumptions are listed below:

1. Storm arrivals are modeled as a poisson process with mean interstorm time λ^{-1} (d).
2. Storm depths are assumed to be independently and identically distributed random variables characterized by an exponential distribution with mean storm depth α (mm).
3. An upper bound, $s \le 1$, is imposed such that saturation-excess runoff occurs whenever the current storm depth is greater than the soil storage capacity.

Under these assumptions, the general form for $p(s)$ is [*Rodriguez-Iturbe et al.*, 1999; *Porporato et al.*, 2004; *Rodriguez-Iturbe and Porporato*, 2004]

$$p(s) = \frac{c}{\rho(s)}\exp\left[-\gamma s - \lambda\int_s^1 \frac{du}{\rho(u)}\right], \tag{A8}$$

where c is a normalization constant and $\gamma = nz_r/\alpha$. Because equation (A3) is bounded at $s = 0$ when $s_e < 0$ (i.e., $k_w + k_s < 1$), $p(s)$ is composed of a continuous part that follows equation (A8) for $s_w < s < 1$ and an atom of probability at $s = 0$, denoted p_0. Following *Rodriguez-Iturbe and Porporato* [2004], the continuous part is given by,

$$p(s) = \frac{c}{\eta}\left(\frac{s-s_e}{1-s_e}\right)^{\frac{\lambda(1-s_e)}{\eta}-1}\exp\left(-\gamma s\right), \tag{A9}$$

and the atom of probability at $s = 0$ is given by

$$p_0 = \frac{\rho(0)p(0)}{\lambda} = \frac{c}{\lambda}\left(\frac{-s_e}{1-s_e}\right)^{\frac{\lambda(1-s_e)}{\eta}-1}\max\left(0, \frac{-s_e}{1-s_e}\right). \tag{A10}$$

where the last term on the right-hand side introduces p_0 only when $s_e < 0$. The normalization constant is obtained by imposing $\int_0^1 p(s)ds = 1 - p_0$,

$$\begin{aligned} c^{-1} = {} & \frac{1-s_e}{\eta}\exp\left(-\gamma s_e\right)\left[\gamma(1-s_e)\right]^{-\frac{\lambda(1-s_e)}{\eta}} \\ & \times\left\{\Gamma\left[\frac{\lambda(1-s_e)}{\eta}, \gamma(s_w - s_e)\right] - \Gamma\left[\frac{\lambda(1-s_e)}{\eta}, \gamma(1-s_e)\right]\right\} \\ & + \frac{1}{\lambda}\left(\frac{-s_e}{1-s_e}\right)^{\frac{\lambda(1-s_e)}{\eta}-1}\max\left(0, \frac{-s_e}{1-s_e}\right) \end{aligned} \tag{A11}$$

©2014. American Geophysical Union. All Rights Reserved.

Appendix B: Soil Moisture Threshold for Carbon Starvation

Below, the condition for mortality by carbon starvation is derived. This is accomplished by expressing the nonstructural carbohydrate (NSC) dynamics in terms of soil moisture and, therefore, deriving the carbon starvation mortality threshold, s_{CS}.

B1. Temporal Dynamics of NSC

The dynamics of NSC (denoted C) are defined by two assumptions. First, when soil moisture exceeds a threshold value s_0, $C = C_0$, the steady state value of NSC where carbon storage is saturated. Second, when soil moisture crosses below s_0, C is depleted in the absence of rainfall according to the following balance of photosynthetic carbon gain and respiratory costs:

$$\frac{dC}{dt} = A_{max} u[s(t), w(t)] - r, \tag{B1}$$

where A_{max} (g C d^{-1}) is the maximum rate of photosynthesis, u is the stomatal control function, and r (g C d^{-1}) is the respiration rate. Integrating equation (B1) with $u[s(t), w(t)]$ given by equations (4), (A6), and (A7), gives

$$C(t) = C_0 + a\tau \left\{1 - \exp\left[-(t - t_{s_0})/\tau\right]\right\} - r(t - t_{s_0}) \tag{B2}$$

where t_{s_0} is the time for s to decay from the initial condition s_i to the threshold s_0 and $a = A_{max}(k_s + k_w\delta)(s_0 - s_e)$. We assume s_0 is the point where respiration exceeds photosynthesis, or $dC/dt = 0$, which gives

$$s_0 = \frac{r}{A_{max}(k_s + k_w\delta)} + s_e. \tag{B3}$$

B2. Carbon Starvation Threshold

Carbon starvation occurs when C reaches a positive threshold, C_c, below which physiological processes cease [*McDowell*, 2011]. This NSC threshold can be translated to a soil moisture threshold using equation (B2) and the results from Appendix A. First, we compute the time to reach C_c from C_0, t_{C_c}, by inverting equation (B2),

$$t_{C_c} = \tau W\left\{-\frac{a}{r}\exp\left[-\frac{(\Delta C + a)}{r\tau}\right]\right\} + \frac{\Delta C + a\tau}{r} \approx \frac{\Delta C + a\tau}{r}, \tag{B4}$$

where $\Delta C = C_0 - C_c$ and $W\{\cdot\}$ is the Lambert W function. It can be shown that the left term in equation (B4) can be neglected for typical parameter values. Therefore, we approximate t_{C_c} with the right term only. Second, the soil moisture threshold for carbon starvation, s_{CS}, is identified using equation (A5),

$$s_{CS} = (s_0 - s_e)\exp\left(-t_{C_c}/\tau\right) + s_e. \tag{B5}$$

Acknowledgments

We acknowledge support from the National Science Foundation (AGS-110227, CBET-1033467, EAR-1013339, EAR-1331846, and EAR-1316258), the United States Department of Agriculture through the Agriculture and Food Research Initiative (2011-67003-30222), and the United States Department of Energy through the Office of Biological and Environmental Research, Terrestrial Ecosystem Science program (DE-SC0006967). We also thank the anonymous reviewers for their helpful comments.

References

Allen, C. D., et al. (2010), A global overview of drought and heat-induced tree mortality reveals emerging climate change risks for forests, *For. Ecol. Manage.*, *259*(4), 660–684, doi:10.1016/j.foreco.2009.09.001.

Amthor, J., and K. McCree (1990), Carbon balance of stressed plants: A conceptual model for integrating research results, in *Stress Responses in Plants: Adaptation and Acclimation Mechanisms*, edited by E. Alscher and J. Cumming, pp. 1–15, Wiley-Liss, New York.

Anderegg, W., J. Berry, D. Smith, J. Sperry, L. Anderegg, and C. Field (2012), The roles of hydraulic and carbon stress in a widespread climate-induced forest die-off, *Proc. Natl. Acad. Sci. U.S.A.*, *109*(1), 233–237, doi:10.1073/pnas.1107891109.

Bechhoefer, J. (2005), Feedback for physicists: A tutorial essay on control, *Rev. Mod. Phys.*, *77*(3), 783–836, doi:10.1103/RevModPhys.77.783.

Breshears, D. D., et al. (2005), Regional vegetation die-off in response to global-change-type drought, *Proc. Natl. Acad. Sci. U.S.A.*, *102*(42), 15,144–15,148, doi:10.1073/pnas.0505734102.

Brodribb, T. J., and S. A. McAdam (2011), Passive origins of stomatal control in vascular plants, *Science*, *331*(6017), 582–585, doi:10.1126/science.1197985.

Buckley, T. N. (2005), The control of stomata by water balance, *New Phytol.*, *168*(2), 275–292, doi:10.1111/j.1469-8137.2005.01543.x.

Clifford, M. J., P. D. Royer, N. S. Cobb, D. D. Breshears, and P. L. Ford (2013), Precipitation thresholds and drought-induced tree die-off: Insights from patterns of Pinus edulis mortality along an environmental stress gradient, *New Phytol.*, *200*(2), 413–421, doi:10.1111/nph.12362.

Davies, W. J., S. Wilkinson, and B. Loveys (2002), Stomatal control by chemical signalling and the exploitation of this mechanism to increase water use efficiency in agriculture, *New Phytol.*, *153*(3), 449–460, doi:10.1046/j.0028-646X.2001.00345.x.

Herms, D. A., and W. J. Mattson (1992), The dilemma of plants: To grow or defend, *Q. Rev. Biol.*, *67*(3), 283–335, doi:10.1086/417659.

©2014. American Geophysical Union. All Rights Reserved.

Katul, G., A. Porporato, and R. Oren (2007), Stochastic dynamics of plant-water interactions, *Annu. Rev. Ecol. Evol. Syst.*, *38*, 767–791, doi:10.1146/annurev.ecolsys.38.091206.095748.

Kumagai, T., and A. Porporato (2012), Strategies of a Bornean tropical rainforest water use as a function of rainfall regime: Isohydric or anisohydric?, *Plant Cell Environ.*, *35*(1), 61–71, doi:10.1111/j.1365-3040.2011.02428.x.

Laio, F., A. Porporato, L. Ridolfi, and I. Rodriguez-Iturbe (2001), Plants in water-controlled ecosystems: Active role in hydrologic processes and response to water stress—II. Probabilistic soil moisture dynamics, *Adv. Water Resour.*, *24*(7), 707–723, doi:10.1016/S0309-1708(01)00005-7.

Magnani, F., J. Grace, and M. Borghetti (2002), Adjustment of tree structure in response to the environment under hydraulic constraints, *Funct. Ecol.*, *16*(3), 385–393, doi:10.1046/j.1365-2435.2002.00630.x.

McDowell, N. (2011), Mechanisms linking drought, hydraulics, carbon metabolism, and vegetation mortality, *Plant Physiol.*, *155*(3), 1051–1059, doi:10.1104/pp.110.170704.

McDowell, N., et al. (2008), Mechanisms of plant survival and mortality during drought: Why do some plants survive while others succumb to drought?, *New Phytol.*, *178*(4), 719–739, doi:10.1111/j.1469-8137.2008.02436.x.

McDowell, N., D. Beerling, D. Breshears, R. Fisher, K. Raffa, and M. Stitt (2011), The interdependence of mechanisms underlying climate-driven vegetation mortality, *Trends Ecol. Evol.*, *26*(10), 523–532, doi:10.1016/j.tree.2011.06.003.

McDowell, N. G., et al. (2013), Evaluating theories of drought-induced vegetation mortality using a multimodel-experiment framework, *New Phytol.*, *200*(2), 304–321, doi:10.1111/nph.12465.

Mitchell, P., A. O'Grady, D. Tissue, D. White, M. Ottenschlaeger, and E. Pinkard (2013), Drought response strategies define the relative contributions of hydraulic dysfunction and carbohydrate depletion during tree mortality, *New Phytol.*, *197*(3), 862–872, doi:10.1111/nph.12064.

Nikinmaa, E., T. Hölttä, P. Hari, P. Kolari, A. Mäkelä, S. Sevanto, and T. Vesala (2013), Assimilate transport in phloem sets conditions for leaf gas exchange, *Plant Cell Environ.*, *36*(3), 655–669, doi:10.1111/pce.12004.

Pantin, F., F. Monnet, D. Jannaud, J. M. Costa, J. Renaud, B. Muller, T. Simonneau, and B. Genty (2013), The dual effect of abscisic acid on stomata, *New Phytol.*, *197*(1), 65–72, doi:10.1111/nph.12013.

Porporato, A., F. Laio, L. Ridolfi, and I. Rodriguez-Iturbe (2001), Plants in water-controlled ecosystems: Active role in hydrologic processes and response to water stress—III. Vegetation water stress, *Adv. Water Resour.*, *24*(7), 725–744, doi:10.1016/S0309-1708(01)00006-9.

Porporato, A., E. Daly, and I. Rodriguez-Iturbe (2004), Soil water balance and ecosystem response to climate change, *Am. Nat.*, *164*(5), 625–632, doi:10.1086/424970.

Rodriguez-Iturbe, I., and A. Porporato (2004), *Ecohydrology of Water-Controlled Ecosystems: Soil Moisture and Plant Dynamics*, Cambridge Univ. Press, New York.

Rodriguez-Iturbe, I., A. Porporato, L. Ridolfi, V. Isham, and D. Cox (1999), Probabilistic modelling of water balance at a point: The role of climate, soil and vegetation, *Proc. R. Soc. London, Ser. A*, *455*(1990), 3789–3805, doi:10.1098/rspa.1999.0477.

Sala, A., F. Piper, and G. Hoch (2010), Physiological mechanisms of drought-induced tree mortality are far from being resolved, *New Phytol.*, *186*(2), 274–281, doi:10.1111/j.1469-8137.2009.03167.x.

Schneider, S. H., et al. (2007), Assessing key vulnerabilities and the risk from climate change, in *Climate Change 2007: Impacts, Adaptation and Vulnerability. Contribution of Working Group II to the Fourth Assessment Report of the Intergovernmental Panel on Climate Change*, edited by M. L. Parry et al., pp. 779–810, Cambridge Univ. Press, Cambridge, U. K.

Sperry, J. S. (2004), Coordinating stomatal and xylem functioning—An evolutionary perspective, *New Phytol.*, *162*(3), 568–570, doi:10.1111/j.1469-8137.2004.01072.x.

Stengel, R. (1994), *Optimal Control and Estimation*, Dover, Mineola, New York.

Tardieu, F., J. Zhang, and D. J. G. Gowing (1993), Stomatal control by both [ABA] in the xylem sap and leaf water status: A test of a model for droughted or ABA-fed field-grown maize, *Plant Cell Environ.*, *16*(4), 413–420, doi:10.1111/j.1365-3040.1993.tb00887.x.

Tardieu, F., T. Lafarge, and T. Simmoneau (1996), Stomatal control by fed or endogenous xylem ABA in sunflower: Interpretation of correlations between leaf water potential and stomatal conductance in anisohydric species, *Plant Cell Environ.*, *19*(1), 75–84, doi:10.1111/j.1365-3040.1996.tb00228.x.

Vandeleur, R. K., G. Mayo, M. C. Shelden, M. Gilliham, B. N. Kaiser, and S. D. Tyerman (2009), The role of plasma membrane intrinsic protein aquaporins in water transport through roots: Diurnal and drought stress responses reveal different strategies between isohydric and anisohydric cultivars of grapevine, *Plant Physiol.*, *149*(1), 445–460, doi:10.1104/pp.108.128645.

©2014. American Geophysical Union. All Rights Reserved.